The Astrophysical Journal, 621:461–472, 2005 March 1

THE TRUNCATED DISK OF COKU TAU/4

Paola D'Alessio,[1] Lee Hartmann,[2] Nuria Calvet,[2] Ramiro Franco-Hernández,[1] William J. Forrest,[3] Ben Sargent,[3] Elise Furlan,[4] Keven Uchida,[4] Joel D. Green,[3] Dan M. Watson,[3] Christine H. Chen,[5] F. Kemper,[6] G. C. Sloan,[4] and Joan Najita[7]

Received 2004 August 4; accepted 2004 November 16

ABSTRACT

We present a model of a dusty disk with an inner hole that accounts for the *Spitzer Space Telescope* Infrared Spectrograph observations of the low-mass pre–main-sequence star CoKu Tau/4. We have modeled the mid-infrared spectrum (between 8 and 25 μm) as arising from the inner wall of a disk. Our model disk has an evacuated inner zone of radius $\sim$10 AU, with a dusty inner "wall" of half-height $\sim$2 AU that is illuminated at normal incidence by the central star. The radiative equilibrium temperature decreases from the inner disk edge outward through the optically thick disk; this temperature gradient is responsible for the emission of the silicate bands at 10 and 20 μm. The observed spectrum is consistent with being produced by Fe-Mg amorphous glassy olivine and/or pyroxene, with no evidence of a crystalline component. The mid-infrared spectrum of CoKu Tau/4 is reminiscent of that of the much older star TW Hya, where it has been suggested that the significant clearing of its inner disk is due to planet formation. However, no inner disk remains in CoKu Tau/4, consistent with the star being a weak-emission (nonaccreting) T Tauri star. The relative youth of CoKu Tau/4 ($\sim$1 Myr) may indicate much more rapid planet formation than typically assumed.

Subject headings: circumstellar matter — infrared: stars — planetary systems: formation — planetary systems: protoplanetary disks — stars: pre–main-sequence

Online material: color figure

1. INTRODUCTION

The formation of planets around young stars is thought to involve the eventual clearing of the natal dusty protoplanetary disks, as planets accrete and sweep out material. Coagulation and accretion processes are expected to occur fastest in inner disk regions, where surface densities are higher and orbital periods are shorter (e.g., Wuchterl et al. 2000 and references therein). An observational signature of inner disk gaps or holes would be the reduction or elimination of emission from hot dust, corresponding to a decrease in the short-wavelength infrared emission.

The low-mass pre–main-sequence star CoKu Tau/4 exhibits a spectral energy distribution (SED) with properties suggesting a substantial dusty disk with an evacuated inner region; strong infrared excess emission is detected at wavelengths $\gtrsim$10 μm, with little or no excess over photospheric fluxes at shorter wavelengths, as shown by observations with the Infrared Spectrograph (IRS) on the *Spitzer Space Telescope* (Forrest et al. 2004). The interpretation is that CoKu Tau/4 has a dusty disk that is mostly cleared of small dust grains inside a radius of 10 AU. The qualitative nature of the SED of CoKu Tau/4 is reminiscent of that of the classical T Tauri stars TW Hya (Calvet et al. 2002; Uchida et al. 2004) and GM Aur (Marsh & Mahoney 1992, 1993; Rice et al. 2003) and the Herbig Ae star HD 100546 (Bouwman et al. 2003). Quillen et al. (2004) suggest that the inner disk hole in CoKu Tau/4 might be produced by a relatively low-mass planet; if this is the case, CoKu Tau/4 is particularly interesting because its relative youth ($\sim$1 vs. 10 Myr for TW Hya; Webb et al. 1999) places severe constraints on planetary formation (e.g., Wuchterl et al. 2000 and references therein).

In this paper we present radiative transfer models of CoKu Tau/4 that account for the IRS spectrum and other constraints on the SED. We confirm our previous estimate of the disk inner radius (Forrest et al. 2004) and show that the observed 10 μm silicate emission feature is likely to be produced in the hot outer layer of the disk "wall" facing the star, without requiring any small dust inside the inner hole. We also comment on the dust compositions consistent with the observations.

2. STELLAR PROPERTIES, EXTINCTION, AND SED

CoKu Tau/4 is a weak-emission T Tauri star (WTTS) of spectral type M1.5 (Cohen & Kuhi 1979) with no detectable short-wavelength (UV) excess and an Hα equivalent width $\sim$1.8 Å (Cohen & Kuhi 1979). We assume a distance of 140 pc to the star, based on its location in the Taurus-Auriga molecular cloud (Kenyon et al. 1994).

To estimate the stellar parameters, we need to quantify the extinction to the star. Cohen & Kuhi (1979) found $A_V = 0.94 \pm 0.29$ from their spectral type determination, adoption of the standard reddening law, and using fluxes from their scanner spectra in wavelength regions near 5400, 6000, and 6700 Å. However, such a low extinction is not consistent with relatively recent observations of near-infrared colors. Kenyon & Hartmann (1995, hereafter KH95) find $J - H = 1.10$, and the Two Micron All Sky Survey (2MASS) catalog yields $J - H = 1.08$, while from

[1] Centro de Radioastronomía y Astrofísica, Apdo. Postal 72-3 (Xangari), 58089 Morelia, Michoacán, Mexico; p.dalessio@astrosmo.unam.mx.
[2] Harvard-Smithsonian Center for Astrophysics, 60 Garden Street, Cambridge, MA 02138.
[3] Department of Physics and Astronomy, University of Rochester, 600 Wilson Boulevard, Rochester, NY 14627-0171.
[4] Center for Radiophysics and Space Research, Cornell University, Space Sciences Building, Ithaca, NY 14853-6801.
[5] National Research Council Resident Research Associate, Jet Propulsion Laboratory, Mail Stop 169-506, California Institute of Technology, 4800 Oak Grove Drive, Pasadena, CA 91109.
[6] Department of Physics and Astronomy, UCLA, 405 Hilgard Avenue, Los Angeles, CA 90095-1562.
[7] National Optical Astronomy Observatory, 50 North Cherry Avenue, Tucson, AZ 85719.

Table A4 of KH95, the unreddened color of an M1.5 star should be $J - H = 0.67$. Using an extinction law with $R_V \sim 3.6$, as indicated by the recent study of Calvet et al. (2004), this would suggest $A_V \sim 3$. The $H-K$ colors suggest slightly larger extinctions, but the latter result is much more sensitive to errors in photometry and extinction laws than the result obtained from the $J-H$ colors.

Recent optical spectra of CoKu Tau/4 from the FAST spectrograph on the Fred L. Whipple 1.5 m telescope on Mount Hopkins (discussed in Kenyon et al. 1998) were inspected. Although conditions were not photometric, comparison with other stars observed on the same night indicate a much redder spectrum than shown by Cohen & Kuhi (1979), roughly consistent with $A_V \sim 3$, in agreement with the values of extinction inferred from 2MASS colors. For the purposes of this paper, we therefore adopt $A_V = 3$. Further optical monitoring of CoKu Tau/4 would be desirable.

Following KH95, we assign a stellar effective temperature of $T_* = 3720$ K to CoKu Tau/4. For $A_V = 3$ we find a stellar luminosity of approximately $L_* = 0.61\ L_\odot$ with an error of order 20% or more given possible variability and the uncertainty in extinction corrections. (According to 2MASS $J = 10.16$, while KH95 cite $J = 10.37$.) Evolutionary tracks from Siess et al. (2000) give a mass of $M_* \sim 0.5\ M_\odot$ and an age of $\sim$1.2 Myr for the central star, while those of Baraffe et al. (1998) give $0.66\ M_\odot$ and 1.6 Myr, respectively. Both ages are consistent with that of the rest of the population of Taurus, $\sim$1–2 Myr (Hartmann 2003).

There are two alternatives for the cause of the high extinction observed toward CoKu Tau/4, either of interstellar/intercloud origin or, if CoKu Tau/4 were an edge-on disk, of local origin. However, edge-on disks are underluminous, because the direct light from the star gets heavily extinguished, so the optical spectrum is stellar scattered light (D'Alessio et al. 1999). This scattered component is fainter than the stellar direct flux, because the scattering region does not cover 4π sr. A correction of $A_V = 3$ applied to this scattered light component would still leave the star underluminous; however, with $A_V = 3$ and its current infrared magnitudes, the properties of CoKu Tau/4 agree with those of the low-mass population of Taurus. In addition, the large contrast between 10 and 20 μm in CoKu Tau/4 is much larger than predicted in high-inclination disks with emission at 10 μm (Pascucci et al. 2004)

We then adopt the hypothesis that the extinction toward CoKu Tau/4 is interstellar/intercloud; the presence of a scattered light nebulosity $\sim 1'$ from CoKu Tau/4 (D. Padgett 2004, unpublished) supports the assumption that it is located in a high-density region of the molecular cloud. With this assumption, the IRS spectrum must also be corrected for extinction. Figure 1 shows the IRS spectrum corrected using two different reddening laws, one proposed by Draine (2003) and the other one by Moneti et al. (2001) based on observations from Lutz (1999) and 10 and 18 μm profiles from Simpson (1991). Between 1.2 and 8 μm, the reddening law proposed by Moneti et al. (2001) agrees, within the uncertainties, with the reddening law recently determined using *Spitzer* IRAC data (Indebetouw et al. 2005). The overall features of the spectrum shown in Forrest et al. (2004) are preserved, namely, a steep, roughly photospheric spectrum shortward of about 8 μm, the weak silicate feature at 10 μm, the steep rise between 14 and 20 μm, and the flattening of the emission to longer wavelengths. The shape of the 10 μm silicate feature is slightly dependent upon the extinction law used. The flux error at each wavelength was derived by taking half of the absolute value of the difference in flux from the spectra

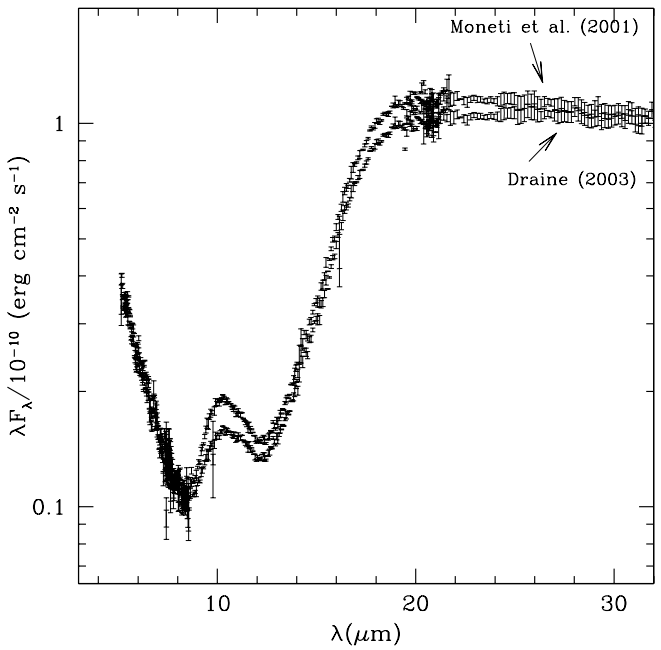

FIG. 1.—Spectrum of CoKu Tau/4 corrected using reddening laws by Draine (2003) and Moneti et al. (2001) assuming $A_V = 3$. The IRS fluxes are shown by error bars, which represent the observed error, estimated as half of the absolute value of the difference in flux from the spectra independently obtained at the two nod positions of the telescope for each order of short-low and long-low.

independently obtained at the two nod positions of the telescope for each order of short-low (SL; 5.2–14 μm, $\lambda/\Delta\lambda \sim 90$) and long-low (LL; 14–38 μm, $\lambda/\Delta\lambda \sim 90$) (see Forrest et al. 2004).

Figure 2 shows fluxes from 2MASS and long-wavelength measurements from the *Infrared Astronomical Satellite* (*IRAS*) from Strom et al. (1989), which may be contaminated by extended emission. For comparison, we show a synthetic stellar spectrum from Bruzual & Charlot (1993) for $T_* = 3720$ K, $R_* = 1.9\ R_\odot$, and $M_* = 0.5\ M_\odot$, along with the median SED of classical T Tauri stars in the Taurus Association (D'Alessio et al. 1999), scaled to the flux in the H band. It is evident that the mid-infrared emission of CoKu Tau/4 is significantly less than those of typical Taurus stars whose disks lack inner holes. In contrast, the flux levels in the 20–35 μm region are relatively bright compared with the median Taurus SED. Our task is to explain this spectrum.

3. MODEL

We have constructed models for CoKu Tau/4 that are similar to the one calculated for TW Hya (Calvet et al. 2002; Uchida et al. 2004). The basic model for TW Hya is that of a fairly massive classical T Tauri disk truncated at an inner radius of about 4 AU (Calvet et al. 2002); at this radius the optically thick disk is frontally illuminated by the central star. A major difference between TW Hya and CoKu Tau/4 is that the former object exhibits clear evidence for gas accretion onto the star (Muzerolle et al. 2000; Batalha et al. 2002). The SED of TW Hya also exhibits a substantial excess at 10 μm and even some small excess emission at wavelengths as short as $\sim$5 μm (Sitko et al. 2000). Calvet et al. (2002) interpreted these results to mean that there is a small amount of optically thin dust and gas interior to the optically thick disk wall, which accounts for the hotter dust emission and the accreting gas. In contrast, CoKu Tau/4 is a

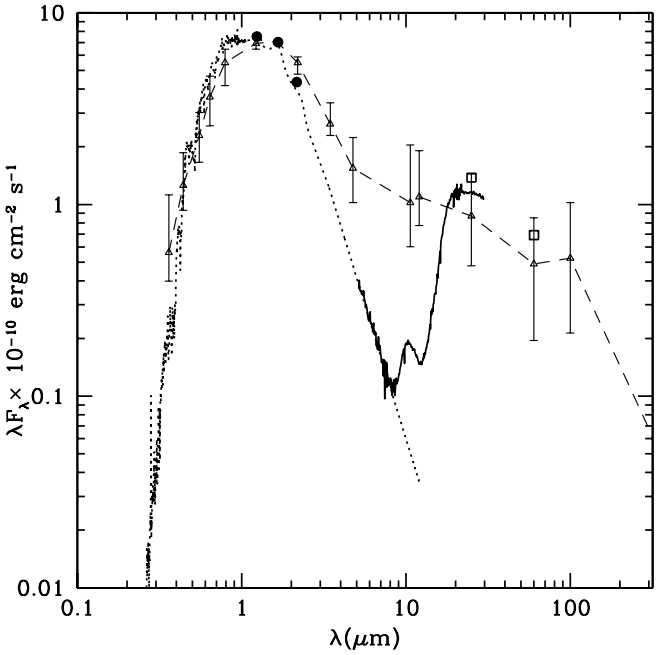

FIG. 2.—Spectral energy distribution of CoKu Tau/4 (*squares*: Strom et al. 1989; *circles*: 2MASS; IRS portion from Forrest et al. 2004) corrected using the reddening law by Moneti et al. (2001) with $A_V = 3$, compared to the median SED of classical T Tauri stars in Taurus (*triangles and dashed line*). The error bars of the median points represent the quartiles (D'Alessio et al. 1999). We also show a synthetic spectrum for the central star taken from Bruzual & Charlot (1993) for $T_* = 3720$ K and $R_* = 1.9\ R_\odot$.

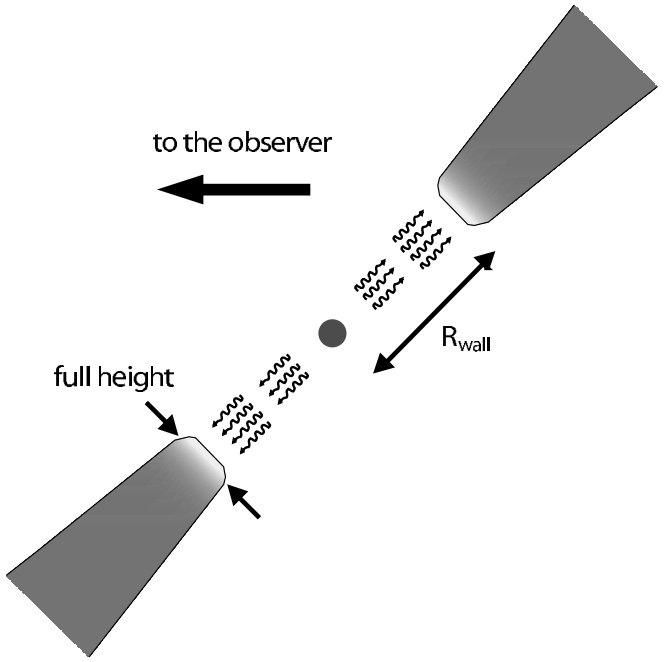

FIG. 3.—Schematic representation of the truncated disk in CoKu Tau/4. [*See the electronic edition of the Journal for a color version of this figure.*]

WTTS with a small Hα equivalent width consistent with stellar chromospheric emission; the accretion rate in this system must be extremely small, if present at all (Muzerolle et al. 2000). In addition, the SED of CoKu Tau/4 is consistent with purely stellar photospheric emission at wavelengths $\lambda \lesssim 8$ μm (Forrest et al. 2004). As discussed in § 2, there are uncertainties at the $\sim$20% level in extrapolating the photospheric continuum from shorter wavelengths to the IRS range; however, the spectral slope at the short-wavelength end of the IRS spectrum is clearly consistent with being purely photospheric, as are IRAC colors of this object between 3.6 and 8 μm (L. Hartmann 2004, private communication).

Thus, we model CoKu Tau/4 as a central star with the properties described in § 2 surrounded by an optically thick, truncated disk with an inner wall at a radius $R_{\rm wall}$. Inside this radius the disk is optically thin; in § 3.4 we estimate the maximum amount of dust in the inner hole or gap consistent with the spectrum. Outside $R_{\rm wall}$ there is a disk, which might contribute to the SED at wavelengths longer than 25 μm. At $R = R_{\rm wall}$ the disk receives radiation frontally from the central star; as we detail in the following, the wall appears to be responsible for most, if not all, of the excess emission detected by IRS.

3.1. *Treatment of the Inner Disk "Wall"*

The wall is the transition between the inner optically thin disk or gap and the outer disk. We assume that it is uniform in the vertical direction and solve its radial structure. Closer to the star, the wall has an optically thin atmosphere, and its radial optical depth increases with radius. Figure 3 shows schematically the structure of this wall.

The temperature distribution of the wall is calculated using the procedure described by Calvet et al. (1991, hereafter CPMD91; 1992), which has been successfully applied to calculate the radial structure of the wall at the dust sublimation radius in disks around classical T Tauri stars by Muzerolle et al. (2003). Since we relax some approximations made in previous papers, we write the equations in detail.

We assume that the stellar radiation penetrates the wall with an angle of zero between the incident direction and the normal to the wall's surface and that the radial thickness of its atmosphere is negligible compared to its distance to the central star. The incident radiation field is separated into two wavelength ranges, one characteristic of the disk (related quantities have subscript d) and one characteristic of the incident stellar radiation (quantities with subscript s). In order to find an analytical solution for the wall radial distribution of temperature, we assume that the opacities are constant in the wall atmosphere and that scattering of stellar radiation is isotropic. We also assume that there is no heating source other than the incident and scattered stellar radiation. At every depth into the wall atmosphere the net outward radial flux at the disk frequency range is equal to the absorbed radiative flux at the stellar frequency range (see CPMD91), i.e., the Eddington flux, H_d, is given by

$$H_d(\tau_s) = \frac{F_0}{4\pi}\alpha\left[(1 + C_1)e^{-\tau_s} + C_2 e^{-\beta\tau_s}\right], \qquad (1)$$

where $\alpha = 1 - w$, w is the mean albedo to the stellar radiation ($w = \sigma_s/\chi_s$), $\beta = (3\alpha)^{1/2}$, $F_0 = L_*/4\pi R_{\rm wall}^2$, and τ_s is the total mean optical depth to the stellar radiation in the incident direction (i.e., along rays parallel to the disk midplane, perpendicular to a cylindrical surface at $R = R_{\rm wall}$). The constants in equation (1) are given by

$$C_1 = -\frac{3w}{1 - \beta^2}, \qquad (2)$$

$$C_2 = \frac{5w}{\beta[1 + (2\beta/3)](1 - \beta^2)}. \qquad (3)$$

The zeroth moment of the transfer equation can be written as (Mihalas 1978)

$$\frac{dH_d}{d\tau_d} = J_d - S_d, \tag{4}$$

where τ_d is the total mean optical depth at the disk frequency range, S_d is the local source function, and J_d is the mean intensity. CPMD91 assume strict LTE, i.e., $S_d = B_d = \sigma_R T_d^4/\pi$, where σ_R is the Stefan-Boltzmann constant. Here we include a term corresponding to the emissivity by scattering at the disk frequency range, i.e.,

$$S_d = (\kappa_d B_d + \sigma_d J_d)/(\kappa_d + \sigma_d), \tag{5}$$

assuming isotropic scattering (Mihalas 1978). With this source function, the zeroth moment of the transfer equation is given by

$$B_d = J_d - \frac{\chi_d}{\kappa_d}\frac{dH_d}{d\tau_d}, \tag{6}$$

where $\chi_d = \kappa_d + \sigma_d$.

Using the Eddington approximation for the disk radiation field, the first moment of the transfer equation is

$$\frac{dJ_d}{d\tau_d} = 3H_d, \tag{7}$$

where we have defined $q = \chi_s/\chi_d$. Integrating J_d from equation (7), using $J_d(0) = 2H_d(0)$ as the boundary condition, and substituting it along with $dH_d/d\tau_d$ from equation (1) into equation (6), the temperature as a function of τ_d can be written as

$$T_d(\tau_d)^4 = \alpha\frac{F_0}{4\sigma_R}\left(C_1' + C_2' e^{-q\tau_d} + C_3' e^{-\beta q\tau_d}\right), \tag{8}$$

where

$$C_1' = (1 + C_1)\left(2 + \frac{3}{q}\right) + C_2\left(2 + \frac{3}{\beta q}\right), \tag{9}$$

$$C_2' = (1 + C_1)\left(\frac{q\chi_d}{\kappa_d} - \frac{3}{q}\right), \tag{10}$$

$$C_3' = C_2\beta\left(\frac{q\chi_d}{\kappa_d} - \frac{3}{q\beta^2}\right). \tag{11}$$

The temperature T_0 at the innermost radius of the wall, at the top of the wall atmosphere where $\tau_d = \tau_s = 0$, can be used to define the wall's radius:

$$R_{\rm wall} = \left[\frac{\alpha L_*}{16\pi\sigma_R}(1 + C_1)\left(2 + q\frac{\chi_d}{\kappa_d}\right) + C_2\left(2 + \beta q\frac{\chi_d}{\kappa_d}\right)\right]^{1/2}\frac{1}{T_0^2}. \tag{12}$$

We use T_0 as an input parameter to characterize the atmosphere of the wall. The value of $R_{\rm wall}$ follows from T_0 and the adopted dust properties using equation (12). The mean opacity in the disk wavelength range is calculated using the Planck function evaluated at T_0 as the weighting function, and the mean opacity in the stellar wavelength range is calculated using the Planck function at T_*. We use Planck means in order to have the correct temperature in the optically thin layers of the wall atmosphere

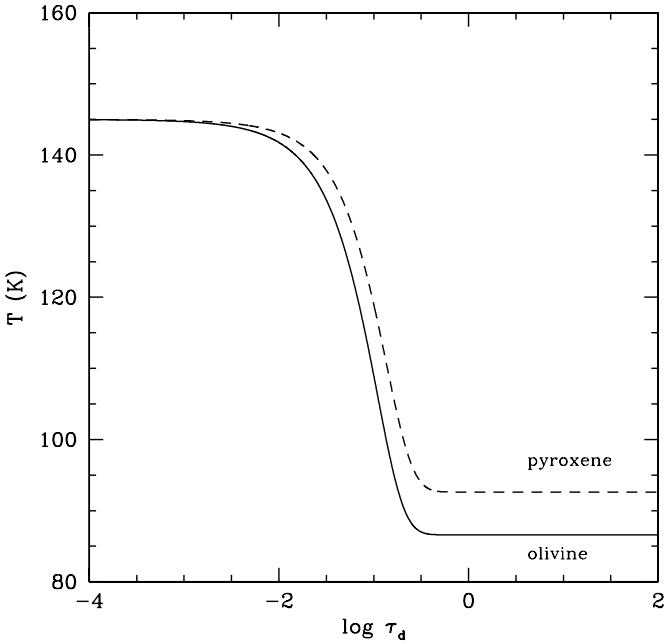

FIG. 4.—Radial distribution of temperature for wall models whose synthetic spectrum fits the observed CoKu Tau/4 spectrum. Both models have $T_0 = 145$ K; one contains $Mg_{0.5}$ $Fe_{0.5}$ olivine (*solid line*) and the other one has $Mg_{0.8}$ $Fe_{0.2}$ pyroxene (*dashed line*) to illustrate the effect of the different silicate compositions on the temperature distribution.

(Mihalas 1978). The minimum temperature of the wall is obtained when $\tau_d \to \infty$, and it is given by

$$T_{\rm min} = \left(\alpha\frac{F_0}{4\sigma_R}C_1'\right)^{1/4}. \tag{13}$$

Figure 4 shows the temperature as a function of the disk mean optical depth (measured from the innermost radius of the wall toward larger radii) for two models with the same value of T_0 but with different kinds of silicates: $Mg_{0.5}$ $Fe_{0.5}$ olivine and $Mg_{0.8}$ $Fe_{0.2}$ pyroxene (in this notation, the subscript to each element represents the fraction of the silicate composed of that element). Both models, with appropriate values for the disk inclination angle and the wall height, reproduce the observed spectrum of CoKu Tau/4 (see § 3.3). The temperature of the wall as a function of optical depth depends on the monochromatic absorption coefficient of the dust through the quantity q, so it has to be calculated for every dust composition attempted to fit the spectrum. However, for a given composition, the temperature is independent of the total dust-to-gas mass ratio, since this ratio affects the heating and the cooling of the grains in the same way, canceling out.

We have calculated the asymmetry factor g for Mg-Fe olivine and pyroxene, the materials that provide the best fit to the observed spectrum (see § 3.3), assuming grains are compact spheres and using the method developed by Wiscombe (1979). We note that the asymmetry factor g of these ingredients decreases with wavelength. In particular, for a maximum grain size $a_{\rm max} = 0.25\ \mu$m, $g \sim 0.6$ for $\lambda = 0.55\ \mu$m, and $g \sim 0.2$ for $\lambda = 1.22\ \mu$m. Taking a Planck mean of the g factor using the Planck function evaluated at the stellar effective temperature as the weighting function, the mean asymmetry factor for the scattering of stellar radiation is $\langle g\rangle \sim 0.3$. This justifies the assumption of isotropic scattering ($g \sim 0$) that we have used to find an analytical solution for the temperature distribution in the disk.

3.2. *Spectrum of the Wall*

Accounting for the limb brightening produced by the temperature inversion in the wall atmosphere, we calculate the emergent intensity for each surface element of the wall as seen in the plane of the sky. The geometry is described in detail in the Appendix. Here we briefly outline the required expressions.

The cosine of the angle between the normal to the surface of the wall and the line of sight is given by

$$\cos\Theta = (\sin i)(\sin\theta), \tag{14}$$

where i is the angle between the disk rotation axis and the line of sight, and θ is such that the coordinate X in the plane of the sky is $X = R_{\rm wall}\cos\theta$. Each element in the visible surface of the wall has a thermal emergent intensity given by

$$I_\nu = \frac{1}{\cos\Theta}\int_0^\infty B_\nu[T_d(\tau_d)]e^{-\tau_\nu/\cos\Theta}\,d\tau_\nu, \tag{15}$$

where $\tau_\nu = \tau_d(\kappa_\nu/\chi_d)$. The emergent flux is calculated by integrating the emergent intensity over the solid angle of the visible surface of the wall. The limits for the integral are given in the Appendix.

Using the intensity given by equation (15) we obtain a limb brightening effect, because rays that pierce the limb of the wall (i.e., $x \sim R_{\rm wall}$; see Fig. 9 below) have an optical depth equal to unity in layers with higher temperature than rays that intersect the wall closer to the center (i.e., $x \sim 0$). This effect would be neglected if the thermal emergent intensity is approximated as isotropic and evaluated at $\cos\Theta = 1$ with the expression

$$I_\nu \approx \int_0^\infty B_\nu[T_d(\tau_d)]e^{-\tau_\nu}\,d\tau_\nu. \tag{16}$$

In this approximation, the emergent flux is calculated by multiplying the total intensity by the total solid angle subtended by the visible side of the wall, which at a distance d from the observer is given by

$$\Omega_{\rm wall} = 2\cos i\left(\frac{R_{\rm wall}}{d}\right)^2\left(\delta\sqrt{1-\delta^2} + \arcsin\delta\right), \quad \text{if } \delta < 1, \tag{17}$$

$$\Omega_{\rm wall} = \pi\left(\frac{R_{\rm wall}}{d}\right)^2\cos i, \quad \text{if } \delta \geq 1, \tag{18}$$

where

$$\delta = \frac{H_{\rm wall}}{R_{\rm wall}}\tan i, \tag{19}$$

and $H_{\rm wall}$ is the (vertical) height of the wall photosphere (measured from the midplane in the vertical direction). Equations (17) and (18) are consistent with the solid-angle portion of the expressions used by Dullemond et al. (2001) to calculate the flux of an isothermal wall.

Limb brightening effects are important when trying to fit a high-resolution spectrum like those of *Spitzer* IRS. For instance, we find that by taking into account limb brightening, the temperature T_0 required to fit the spectrum is 5 K lower than the one in the approximated solution, increasing the wall radius by 10%. In turn, this translates into a height of the wall 20% smaller than the one inferred for the approximated solution. Even more important, the shape of the 20 μm region of the spectrum only can be fitted with the detailed model; the approximated model shows an emission deficit for all the compositions we have tried (described in § 3.3). The 20 μm flux deficit of the approximated model compared to the observed spectrum could be wrongly interpreted as the lack of additional unknown opacity sources.

3.3. *Dust Properties*

We use a mixture of grains composed of silicates with mass fraction $\zeta_{\rm sil} = 0.0034$, organics with $\zeta_{\rm org} = 0.001$, and troilite with $\zeta_{\rm troi} = 7.68\times10^{-4}$. The grains are assumed to be spheres. We adopt the standard MRN grain size distribution $n(a) \sim a^{-3.5}$ (Mathis et al. 1977) between minimum radius $a_{\rm min}$ and maximum radius $a_{\rm max}$. The opacity is calculated using the Mie theory with a code developed by Wiscombe (1979). Optical constants for the organics are taken from Pollack et al. (1994) and for troilite from Pollack et al. (1994) and Begemann et al. (1994). Sublimation temperatures $T_{\rm sil} = 1400$ K, $T_{\rm org} = 425$ K, and $T_{\rm troi} = 680$ K are adopted.

The shape of the 10 μm silicate band and the position of the peak in the spectrum of CoKu Tau/4 indicates that the grains responsible for the emission are small. We adopt $a_{\rm min} = 0.005$ μm and $a_{\rm max} = 0.25$ μm, which are consistent with ISM grains (Draine & Lee 1984). If grains were larger than this, then the peak of the silicate emission would broaden to longer wavelengths than observed.

We have considered several possibilities for the composition of the silicates (see Henning et al. 1999[8]). The observed 10 μm band is smooth and narrow, with no evidence of the substructure characteristic of crystalline components such as enstatite, forsterite, and silica (e.g., Uchida et al. 2004), suggesting the silicates should be glassy and amorphous. In particular, the shape of the observed 10 μm band allows us to rule out glassy bronzite (with optical constants from Dorschner et al. 1988), crystalline bronzite (optical constants from Henning & Mutschke 1997), crystalline silicates of mean cosmic composition $Mg_{0.50}\,Fe_{0.43}\,Ca_{0.03}\,Al_{0.04}\,SiO_3$ (optical constants from Jäger et al. 1994), oxygen-rich and oxygen-deficient circumstellar silicates (optical constants from Ossenkopf et al. 1992), and the absorption coefficient proposed by Draine (2003)[9] for interstellar medium dust. The Draine (2003) mixture and the oxygen-rich and -deficient circumstellar silicates from Ossenkopf et al. (1992) produce an excess flux at the 10–13 μm wavelength range and a deficit at longer wavelengths compared to the CoKu Tau/4 spectrum. The model spectrum calculated for glassy silicates of mean cosmic composition $Mg_{0.50}\,Fe_{0.43}\,Ca_{0.03}\,Al_{0.04}\,SiO_3$ (optical constants from Jäger et al. 1994) fits well the 10 μm band, but the shape of the spectrum between 20 and 30 μm is different from the observed one. Figure 5 shows that some examples of the synthetic spectra of models that we have considered do not fit the observed spectrum. It is important to mention that we have changed the temperature T_0, inclination angle, and height of the wall in the ranges described below, and we have not found any combination of parameters for these compositions that produces a good fit to the observed spectrum.

On the other hand, amorphous Mg-Fe glassy olivine ($Mg_{0.5}\,Fe_{0.5}\,SiO_4$) and glassy pyroxene (in particular, $Mg_{0.95}\,Fe_{0.05}\,SiO_3$ and $Mg_{0.8}\,Fe_{0.2}\,SiO_3$) with optical constants from Dorschner

[8] See http://www.astro.uni-jena.de/Laboratory/Database/jpdoc/index.html.
[9] See http://www.astro.princeton.edu/~draine/dust/dustmix.html.

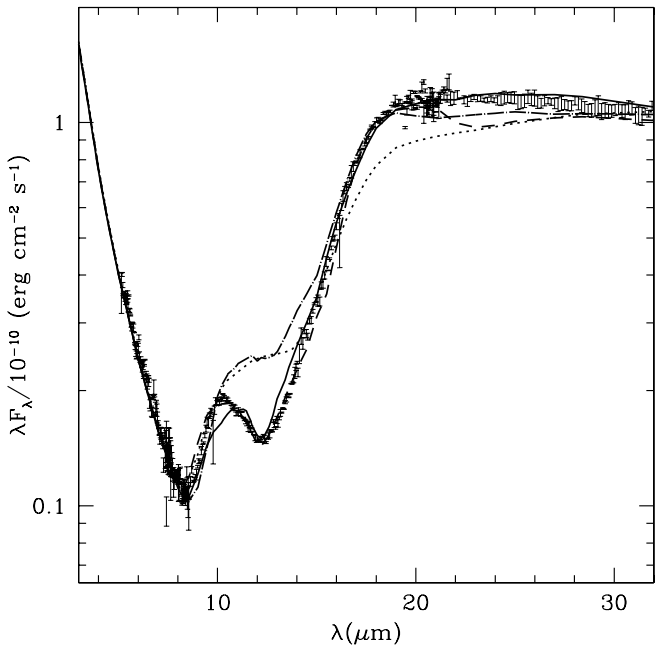

FIG. 5.—Spectra of wall models calculated using different optical constants: silicates from Draine (2003) (*dotted line*) for $H_{\rm wall} = 280\ R_*$; glassy silicates of mean cosmic composition $Mg_{0.50}\ Fe_{0.43}\ Ca_{0.03}\ Al_{0.04}\ SiO_3$ (*dashed line*) with optical constants from Jäger et al. (1994) and $H_{\rm wall} = 240\ R_*$; glassy bronzite (*solid line*) with optical constants from Dorschner et al. (1988) and $H_{\rm wall} = 240\ R_*$; oxygen-rich circumstellar silicates (*dot-dashed line*) with optical constants from Ossenkopf et al. (1992) and $H_{\rm wall} = 320\ R_*$. In all these models $T_0 = 145$ K and $\cos i = 0.55$. The synthetic spectra are compared to the spectrum of CoKu Tau/4 corrected using the Moneti et al. (2001) reddening law.

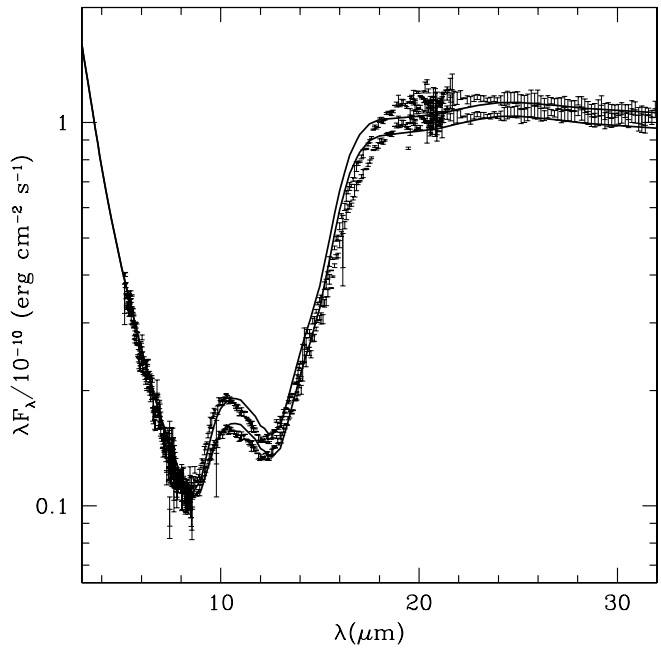

FIG. 6.—Examples of wall model spectra (*solid lines*) that fit the observed spectrum of CoKu Tau/4 corrected by the reddening laws of Draine (2003) (model parameters: $T_0 = 140$ K, $\cos i = 0.45$, and $H_{\rm wall} = 280\ R_*$) and Moneti et al. (2001) (model parameters: $T_0 = 145$ K, $\cos i = 0.45$, and $H_{\rm wall} = 260\ R_*$). The dust consists of small grains ($a_{\rm max} = 0.25\ \mu$m) of glassy olivine with 50% Fe and 50% Mg and with a small amount of organic and troilite grains (see § 3.3).

et al. (1995) produce a reasonable fit to the spectrum. In particular, the pyroxene has a broader 10 μm band than the observed one but fits the spectrum for $\lambda > 18\ \mu$m better than the olivine. On the other hand, the shape of the 10 μm band predicted for the olivine is in better agreement with the observed spectrum. We find that if olivine or pyroxene has less magnesium, then the resulting model spectrum has a flatter 10 μm band compared to the observed one. However, we are not considering both olivine and pyroxene nor the effect of the grains' shape and porosity, which could affect the shape of the bands. Thus, given the errors and our limited set of compositions, we only conclude that both glassy olivine and glassy pyroxene can be present in the wall of CoKu Tau/4 and that there is no evidence of a crystalline component. Figures 6 and 7 show examples of the model spectra calculated for each of these ingredients that fit the observed spectrum reasonably well.

For each grain composition, we calculate the temperature distribution using equation (8) and, in order to fit the observed spectrum, we vary the disk inclination angle and the height of the wall, which are properties not constrained by other means. Thus, for each composition we have calculated a small grid of wall models for $T_0 = 130$, 135, 140, 145, 150, 155, and 160 K, $\cos i = 0.25$, 0.35, 0.45, 0.55, 0.65, and 0.75, $H_{\rm wall} = 200$, 220, 240, 260, 280, and 300 R_* (i.e., 1.77, 1.95, 2.13, 2.3, 2.48, and 2.66 AU). Assuming that gas and dust have the same temperature at the wall, we can evaluate a characteristic vertical gas scale height as $h_{\rm wall} = c_s(T_0)/\Omega_k(R_{\rm wall}) = 1.05(T_0/140\ {\rm K})^{1/2}\ (R/10\ {\rm AU})^{3/2}$; thus, the wall height we are testing spans from 1.5 to 2.5 times $h_{\rm wall}$. The values of $H_{\rm wall}/h_{\rm wall}$ are consistent with the height for which the optical depth to the stellar radiation becomes unity times the local gas scale height at $\sim$10 AU in a nontruncated accretion disk.

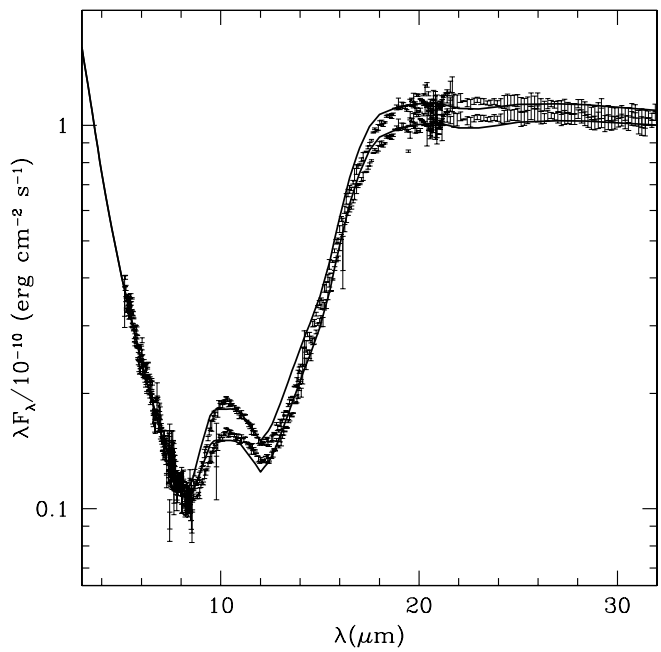

FIG. 7.—Example of wall model spectra (*solid lines*) that fit the observed spectrum of CoKu Tau/4 corrected by the reddening laws of Draine (2003) (model parameters: $T_0 = 140$ K, $\cos i = 0.45$, and $H_{\rm wall} = 240\ R_*$) and Moneti et al. (2001) (model parameters: $T_0 = 145$K, $\cos i = 0.45$, and $H_{\rm wall} = 240\ R_*$). The dust consists of small grains ($a_{\rm max} = 0.25\ \mu$m) of glassy pyroxene with 20% Fe and 80% Mg and with a small amount of organic and troilite grains (see § 3.3).

TABLE 1
PARAMETERS FOR THE WALL

	Moneti et al.'s Law				Draine's Law			
Silicates	T_0 (K)	R_{wall} (AU)	cos i	H_{wall}/R_{wall}	T_0 (K)	R_{wall} (AU)	cos i	H_{wall}/R_{wall}
olmg50	145	11.0	0.35	0.22/0.24	140	12.1	0.35	0.20/0.22
	...	...	0.45	0.21/0.22	...	...	0.45	0.2/0.22
	...	...	0.55	0.21/0.22	...	...	0.55	0.20
	...	...	0.65	0.22	...	...	0.65	0.20
	150	10.1	0.35	0.21	145	11.0	0.25	0.21/0.22
	...	...	0.45	0.21	...	...	0.35	0.19/0.21
	...	...	0.55	0.21	...	...		
pyrmg95	140	10.3	0.45	0.24	140	10.3	0.35	0.22
	...	...	0.55	0.24/0.26	...	...	0.45	0.21
	...	...	0.65	0.24	...	...	0.55	0.21/0.22
	145	9.4	0.25	0.28	...	...	0.65	0.21/0.22
	...	...	0.35	0.23/0.24	...	...	0.75	0.22
	...	...	0.45	0.23/0.24	145	9.3	0.25	0.21
	...	...	0.55	0.23	...	...	0.35	0.19/0.21
	...	...	0.65	0.23	...	...	0.45	0.19
	150	8.6	0.25	0.23/0.25	...	...	...	...
	...	...	0.35	0.21	...	...	...	...
	...	...	0.45	0.21	...	...	...	...
pyrmg80	140	10.4	0.35	0.25	135	11.4	0.45	0.23
	...	...	0.45	0.24	...	...	0.55	0.23
	...	...	0.55	0.24	140	10.4	0.25	0.24/0.25
	...	...	0.65	0.25	...	...	0.35	0.22
	145	9.4	0.35	0.23/0.24	...	...	0.45	0.20/0.22
	...	...	0.45	0.23	...	...	0.55	0.20
	...	...	0.55	0.23	...	...	0.65	0.22
	150	8.7	0.35	0.20/0.22	...	...	0.75	0.22
	...	...	...	...	145	9.4	0.25	0.23
	...	...	...	...	...	...	0.35	0.19/0.21
	...	...	...	...	...	...	0.45	0.19
	...	...	...	...	...	...	0.55	0.19

NOTE.—In this table, olmg50 refers to $Mg_{0.5}$ $Fe_{0.5}$ SiO_4, pyrmg95 to $Mg_{0.95}$ $Fe_{0.05}$ SiO_3, and pyrmg80 to $Mg_{0.8}$ $Fe_{0.2}$ SiO_3.

Table 1 summarizes the parameters that best fit the observed spectrum for each composition and for the two different reddening laws from Draine (2003) and Moneti et al. (2001). Given the uncertainties in the reddening law, dust composition, and disk inclination angle, we can conclude that the hole has a radius R_{wall} between 9 and 12 AU, or $R_{wall} = 10.5 \pm 1.5$ AU, corresponding to a maximum temperature in the atmosphere of the wall between 140 and 150 K. If the Draine (2003) reddening law is used or the silicate dust is dominated by olivine, the resulting wall is slightly colder and farther away than when the Moneti et al. (2001) law is used or the dust is dominated by pyroxene. In each case, a different set of disk inclination angles and wall heights are required to fit the observed spectrum. The inclination angle is not well constrained from the comparison between the observed and the synthetic spectra; however, for different compositions, inclination angles, temperatures, and reddening laws, we have a robust estimate of the height of the wall relative to its radius, $H_{wall}/R_{wall} \approx 0.22 \pm 0.02$.

3.4. *Limits on Dust in the Inner Disk*

In this section we quantify an upper limit of the dust mass in the inner hole of CoKu Tau/4. The dust mean temperature is calculated assuming radiative equilibrium between the dust grains and the stellar radiation field. We assume the inner hole, filled with gas and small grains, has a constant optical depth at 10 μm (measured from the midplane to the surface of the disk) as a function of radius. The dust mass in the inner disk is given by

$$M_{sil}^{hole} \approx 6.6 \left(\frac{\tau_{10\,\mu m}}{\kappa_{10\,\mu m}}\right)\left(\frac{\zeta_{sil}}{0.0034}\right)\left(\frac{R_{wall}}{10\ \mathrm{AU}}\right)^2 \text{ lunar masses.} \quad (20)$$

For $Mg_{0.5}$ $Fe_{0.5}$ SiO_4 olivine, with $a_{max} = 0.25$ μm, the absorption coefficient at the 10 μm peak is $\kappa_{10\,\mu m} = 9$ cm^2 g^{-1}, assuming a silicate dust-to-gas mass ratio $\zeta_{sil} = 0.0034$. Thus, for $\tau_{10\,\mu m} = 0.01$ and a wall radius $R_{wall} \sim 10$ AU, the silicate mass in the inner hole is 0.007 lunar masses.

The left panel of Figure 8 shows the contribution to the SED of the dust in the hole (assuming a sublimation temperature $T_{sil} = 1400$ K) for different values $\tau_{10\,\mu m}$. The temperature of the hottest dust grains inside this inner hole is such that the emissivity is larger at 10 μm than at 20 μm, in contrast to the observed spectrum. The only way to compensate for this effect is to assume a particular radial dependence of $\tau_{10\,\mu m}$, for instance, if $\tau_{10\,\mu m}$ is very small in the hole and increases rapidly at $R \sim R_{wall}$ (which is precisely how the wall is defined). For these small grains, we find that the upper limit of the silicate mass in the inner disk is $M_{sil}^{hole} < 0.0007$ lunar masses. A higher mass than this limit would distort the 10 μm silicate band.

The right panel of Figure 8 illustrates the effect of increasing the maximum grain size. For a fixed value of the optical depth at

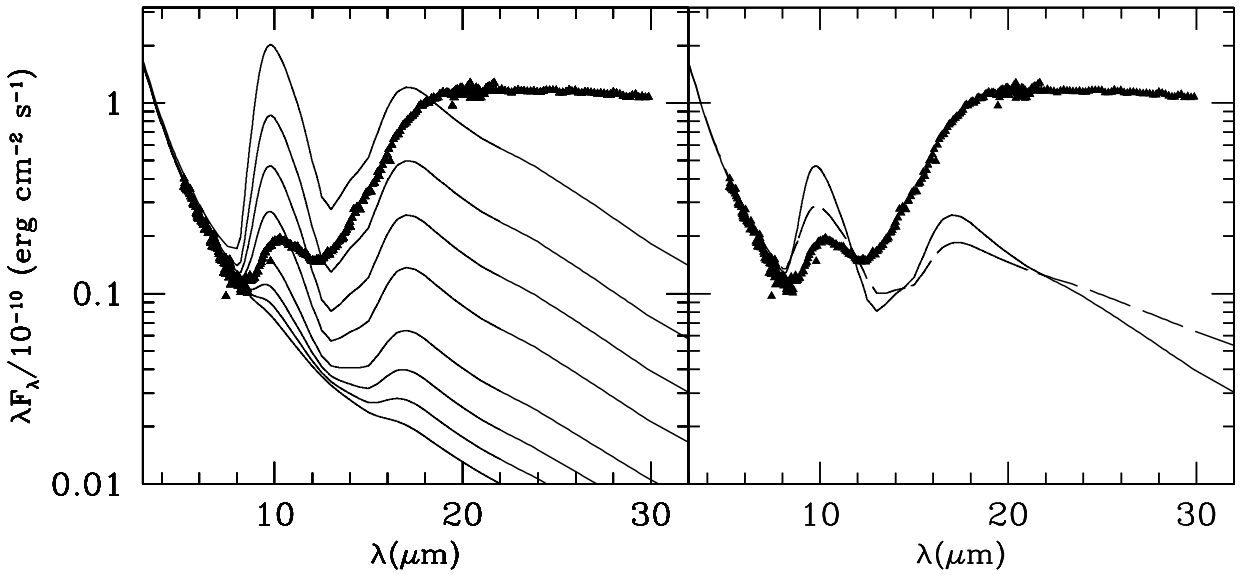

FIG. 8.—Spectrum of dust in the inner disk compared with the IRS spectrum of CoKu Tau/4 corrected using the reddening law by Moneti et al. (2001). The adopted dust is composed of glassy olivine with 50% Fe and 50% Mg. *Left*: For $a_{\max} = 0.25$ μm; each curve corresponds to a different total silicate mass $M_{\rm sil}^{\rm hole} = 0.00015$, 0.0004, 0.0007, 0.0015, 0.004, 0.007, 0.015, and 0.04 lunar masses (corresponding to $\tau_{10\ \mu{\rm m}} = 0.0002$, 0.0005, 0.001, 0.002, 0.005, 0.01, 0.02, 0.05, *bottom to top*). *Right*: For $\tau_{10\ \mu{\rm m}} = 0.01$; each curve corresponds to a different maximum grain size $a_{\max} = 0.25$ (*solid line*) and 10 (*long-dashed line*) (corresponding to $M_{\rm sil}^{\rm hole} = 0.007$ and 0.013 lunar masses, respectively). Bigger maximum grain sizes, for the same optical depth at 10 μm, produce a similar spectrum to the case for $a_{\max} = 10$ μm but for a different total dust mass. For instance, $a_{\max} = 1$ cm corresponds to 0.36 lunar masses, $a_{\max} = 1$ m to 3.6 lunar masses. In each of these cases, $a_{\min} = 0.005$ μm and the exponent of the size distribution is $p = 3.5$.

10 μm, $\tau_{10\ \mu{\rm m}} = 0.01$, we show the spectrum of the interior for different maximum grain sizes. Since the absorption coefficient at 10 μm decreases with $a_{\max}$, each spectrum corresponds to a different silicate mass. If grains are larger, the mass limit increases. For instance, if the grains in the inner hole have $a_{\max} = 10$ μm, then $M_{\rm sil}^{\rm hole} < 0.0013$ lunar masses.

There are not enough constraints on the properties of the whole disk, but speculating that before the gap formation it was a typical α-irradiated disk with $\dot{M} = 10^{-8}\ M_\odot\ {\rm yr}^{-1}$ and $\alpha = 0.01$, the gas mass of the unperturbed inner region (for $R < 10$ AU) is $M_{\rm gas} = 3 \times 10^{-3}\ M_\odot$. For the adopted silicate dust-to-gas mass ratio, one would expect to find $M_{\rm sil}^{\rm hole} = 250$ lunar masses in the hole. The lost mass in grains could be locked in larger bodies or could have been accreted by the star. In the first case, bodies would have grown to ~30 km to account for this mass, assuming that the same power law holds even for this huge size.

3.5. *The Outer Disk Contribution*

Given the uncertainty of the flux at 60 μm and that there is only an upper limit for the flux at 1.3 mm ($F_\nu < 15$ mJy; Osterloh & Beckwith 1995), it is difficult to constrain the outer disk.

The wall treatment assumes plane-parallel geometry. We therefore estimate that the heated wall region has a radial thickness $\Delta R \lesssim H_{\rm wall}$, where $H_{\rm wall}$ is the thickness of the wall photosphere. Then, measured either radially or vertically,

$$\tau_d \sim \kappa_d \Sigma. \tag{21}$$

If we estimate $\kappa_d \sim 2$ cm^2 g^{-1} (see § 3.3), then

$$\tau_d \sim \Sigma. \tag{22}$$

Our disk models with typical parameters for T Tauri stars ($\dot{M} \sim 10^{-8}\ M_\odot\ {\rm yr}^{-1}$, $\alpha = 0.01$) yield $\Sigma \sim 10$ g cm^{-2} at 10 AU, so $\tau_d \sim 10$, consistent with our optically thick wall treatment but low enough not to contribute significantly at 1.3 mm (the mass of the wall is only $\sim 10^{-4}\ M_\odot$). Of course, the disk structure might be quite different, with a pileup of material at the disk wall (a ring); in this case we can limit the amount of mass present, depending upon the adopted opacity, assuming that the wall and the disk are optically thin, taking the Rayleigh-Jeans limit, and taking the minimum temperature of the wall, $T_{\min} \sim 85$ K (eq. [13]) as the maximum temperature of the disk:

$$\frac{M_{\rm disk}}{0.001\ M_\odot} < \left(\frac{F_\nu}{15\ {\rm mJy}}\right)\left(\frac{\kappa_{1.3\ {\rm mm}}}{0.01\ {\rm cm}^2\ {\rm g}^{-1}}\right)^{-1}\left(\frac{T_{\min}}{85\ {\rm K}}\right)^{-1}, \tag{23}$$

where the adopted opacity corresponds to a maximum grain size ~1 mm. Smaller or bigger maximum grain sizes would imply a higher mass given the same flux. To better constrain the outer disk, it would be very useful to measure the fluxes at 70 μm and longer wavelengths.

4. ORIGIN OF THE HOLE IN CoKu TAU/4

What is the origin of the central clearing in the CoKu Tau/4 disk? Processes such as grain coagulation and disk accretion are expected to play a role in preferentially reducing the opacity of the inner disk relative to the outer disk due to both the high surface densities and shorter orbital periods in this region. So, as alluded to earlier (see § 3.4), a possible explanation for the observed SED is that grain growth has led to the production of bodies up to 30 km in size, rendering the inner disk optically thin. Whether or not models of disk accretion and grain growth can reproduce in detail the observed SED of CoKu Tau/4 is an interesting topic for future study.

In the context of the model presented here, we show that the observed SED of CoKu Tau/4 is consistent with a dramatic decrement in the dust opacity at a radial distance of 10 AU. An

interesting interpretation of this structure is that the growth of large bodies has reached an advanced state, producing a planet with a mass large enough to open a substantial gap, allow the interior material to accrete onto the star, and prevent through orbital resonances the progress toward the star of disk material farther out. This effect has been suggested as the reason for central clearings in disks around T Tauri stars (e.g., Marsh & Mahoney 1992, 1993) and debris disks (Jura et al. 1993; Backman et al. 1986). We consider this also to be the most probable origin for the clearing in CoKu Tau/4; in fact, the case for planet formation is somewhat stronger than in the older systems after considering several alternatives as follows.

Radiation pressure or Poynting-Robertson effect.—In an optically thin disk of this size, the lifetime of dust grains 10 AU from a star like CoKu Tau/4 due to these effects would be about 10^5 yr (see, e.g., Chen & Jura 2001; Burns et al. 1979). In a disk that is optically thick to most of the starlight, the timescales are substantially longer ($\gg$1 Myr), as the material would have to be removed an optical depth at a time. The outer disk of CoKu Tau/4 is quite optically thick even in the mid-infrared; so are the inner disks around most other classical T Tauri stars. Thus, these effects are very unlikely to be important here. Even if they were, they would not naturally lead to a very sharp edge.

Sharp change in gravitational field at 10 AU (see Duschl 1989).—This effect, which has been invoked to explain the central clearings in galactic nuclei, could be used here if the disk were self-gravitating at $r > 10$ AU; the inner part would fall in and be accreted by the star on the viscous timescale ($\sim 10^5$ yr; Quillen et al. 2004). However, the limit on the mass of the CoKu Tau/4 disk from millimeter-wave observations (Osterloh & Beckwith 1995), $10^{-3}\ M_\odot$, is too small for the disk to be self-gravitating.

Radial grain segregation.—In debris disks around A stars young enough for some gas still to be present, it has been predicted that the combined effects of radiation pressure and gas drag would lead to central clearings in the distribution of small grains (Takeuchi & Artymowicz 2001). The radiative requirements are similar to those of radiation pressure and Poynting-Robertson drag, though; in the present case the disk is too optically thick and the star too cool for this process to produce a central clearing within 1 Myr.

Stellar companion.—Were CoKu Tau/4 to have a stellar or planetary companion, a clear gap would be produced on timescales shorter than the 1 Myr stellar age if the accretion timescale were sufficiently short and if the companion were sufficiently massive both to open a gap in the disk (i.e., if its Hill radius were to exceed the original half-density thickness of the disk) and to prevent migration. Accretion of the inner-disk material would take place on the viscous timescale of 10^5 yr, which is indeed sufficiently short. A terrestrial-size planet would be unable to produce a gap or prevent migration. A stellar companion could do both. No such companion has yet been observed. The visible and infrared properties of CoKu Tau/4 are accurately consistent with a single M1.5 pre–main-sequence star; a companion star is constrained to have a luminosity of at most a small fraction of that of the M1.5 star, for which the luminosity is already small on the scale of stars. Thus, it is not impossible that the central clearing has been produced and maintained by a very low-mass star that has so far escaped detection. The range of stellar masses for this to work is so narrow, however, that this seems less likely an option than a substellar companion.

A companion in a wide range of masses in the giant planet or brown dwarf regime would produce such an empty, sharp-edged clearing as we see. Upon formation of the companion, material farther out than the strongest orbital resonances would be held up by frequent collisions at these resonances until the mass held up were similar to the mass of the companion. Material inside these resonances would simply be accreted on the viscous timescale. Quillen et al. (2004) have recently simulated the dynamics of a CoKu Tau/4–like disk that undergoes giant-planet formation and found that clearings like the one observed were produced for companions as small as 0.1 Jupiter masses.

Observations can be used to test the scenario proposed in this paper to interpret the spectrum of CoKu Tau/4. For instance, molecular line observations could probe whether the outer disk is gaseous; continuum millimeter observations can be used to quantify the outer disk mass; spatially resolved images could confirm that there is a sharp decline in the dust column density around 10 AU and might reveal whether the disk has the nonaxisymmetric structure that is expected to be induced by the planet (e.g., Quillen et al. 2004).

5. DISCUSSION AND SUMMARY

The spectrum of CoKu Tau/4 is consistent with that expected from a disk truncated at an inner radius of $\sim$10 AU. No detectable material is in the inner hole; the spectrum indicates at most 0.0007 lunar masses of small silicate grains in the inner hole region. Even though CoKu Tau/4 is much younger than TW Hya, the hole in its inner disk is larger and apparently more evacuated of dust and gas (judged by the lack of near-infrared dust emission and gaseous accretion), and its outer disk appears to be much less massive. This comparison clearly indicates that age is not the sole parameter in determining disk evolution. That other parameters influence the properties of pre–main-sequence disks has been clear for some time. For example, nearly half the stars in Taurus lack inner disks, some (but not necessarily all) of which can be explained by the presence of perturbing binary companions (e.g., Mathieu et al. 2000 and references therein).

Because it seems likely that even binary systems once possessed accretion disks (see, e.g., Bate et al. 2003), there must be a wide range of evolutionary timescales for protoplanetary disks. The reasons for this range of timescales are not clear, but we conjecture that initial angular momentum could play a crucial role; disks of similar mass but much smaller initial radii are more likely to fragment and to coagulate faster (given higher initial disk surface densities). This conjecture predicts that the outer radius of the CoKu Tau/4 disk is small; observational efforts to explore this possibility should be made. In any case, given the low disk mass estimate, CoKu Tau/4 may be a system observed just barely before the initial disk material disappears.

Finally, to summarize our results, we find that an inner disk wall at $R \sim 10$ AU with a half-height $H_{\rm wall} \sim 2$ AU is responsible for the observed excess between 8 and 30 μm. This inner wall has an optically thin atmosphere closer to the star, with a temperature decreasing with radius. The highest temperature of the wall is $\sim$145 K, but it decreases rapidly to $\sim$85 K in the deepest layers. Both the 10 and 20 μm bands emerge from the optically thin hotter layers. The spectrum for $\lambda > 20$ μm emerges from the optically thick layers of the wall. At even longer wavelengths the whole wall becomes optically thin, and it is expected that the outer disk dominates the SED. Using an upper flux limit at 1.3 mm (Osterloh & Beckwith 1995) and assuming that the wall is so optically thin at this wavelength that it does not contribute to the flux, we estimate the mass of the outer disk to be less than $0.001\ M_\odot$ for a maximum grain size of 1 mm. The central star dominates the spectrum at $\lambda < 8$ μm.

From an analysis of the 10 μm feature, we find that most of the dust in the wall should be glassy Fe-Mg olivine and/or pyroxene, with no evidence of a crystalline component. We believe this

represents the initial, unprocessed state of the dust in the disk that formed around CoKu Tau/4.

This work is based on observations made with the *Spitzer Space Telescope*, which is operated by the Jet Propulsion Laboratory, California Institute of Technology under NASA contract 1407. Support for this work was provided by NASA through contract 1257184 issued by JPL/Caltech and through the Spitzer Fellowship Program, under award 011 808-001. P. D. and R. F. H. acknowledge grants from CONACyT and DGAPA. N. C. and L. H. acknowledge support by NSF grant AST99-87367 and NASA grant NAG5-10545. F. K. acknowledges support provided by NASA through the Spitzer Fellowship Program, under award 011 808-001.

APPENDIX

The (x, y, z) coordinate system is centered on the star; the z axis is the disk rotation axis, and the (x, y) plane is the disk midplane. We also use cylindrical coordinates R, θ, and z. The wall is a cylinder with radius $R_{\rm wall}$ and total height $2H_{\rm wall}$. Points on the wall surface have coordinates $z, x = R_d \cos\theta$ and $y = R_d \sin\theta$. We use another coordinate system, (X, Y, Z), also centered on the star, where Z is along the line of sight and (X, Y) is the plane of the sky. Both systems coincide when the disk is pole-on. The transformation between coordinate systems is

$$x = X, \tag{24}$$

$$y = Y\cos i - Z\sin i, \tag{25}$$

$$z = Y\sin i + Z\cos i \tag{26}$$

or

$$X = x, \tag{27}$$

$$Y = y\cos i + z\sin i, \tag{28}$$

$$Z = z\cos i - y\sin i. \tag{29}$$

The normal to the cylinder's farthest wall (which is the one the observer will see) is

$$\hat{\boldsymbol{n}} = -\hat{\boldsymbol{R}} = -(\cos\theta)\hat{\boldsymbol{x}} - (\sin\theta)\hat{\boldsymbol{y}}; \tag{30}$$

thus, the cosine between the line of sight

$$\hat{\boldsymbol{Z}} = -(\sin i)\hat{\boldsymbol{y}} + (\cos i)\hat{\boldsymbol{z}} \tag{31}$$

and the normal to the visible surface of the wall is

$$\cos\Theta = \hat{\boldsymbol{Z}}\cdot\hat{\boldsymbol{n}} = (\sin i)(\sin\theta). \tag{32}$$

A surface element of the visible area is $dA = dX\,dY = -R_d \sin\theta\, d\theta\, dY$. To find the limits of the visible surface, we have to define two ellipses (given by the projections of the upper and lower tops of the wall; see Fig. 9). For the upper ellipse

$$\frac{Y_{\rm up}}{R_d} = \pm(\cos i)\sqrt{1 - \frac{X^2}{R_d^2}} + \frac{H}{R_d}\sin i. \tag{33}$$

For the lower ellipse

$$\frac{Y_{\rm down}}{R_d} = \pm(\cos i)\sqrt{1 - \frac{X^2}{R_d^2}} - \frac{H}{R_d}\sin i, \tag{34}$$

which also can be written in terms of θ, using $X = x = R_d\cos\theta$,

$$\frac{Y_{\rm up}}{R_d} = \pm(\cos i)(\sin\theta) + \frac{H}{R_d}\sin i, \tag{35}$$

$$\frac{Y_{\rm down}}{R_d} = \pm(\cos i)(\sin\theta) - \frac{H}{R_d}\sin i. \tag{36}$$

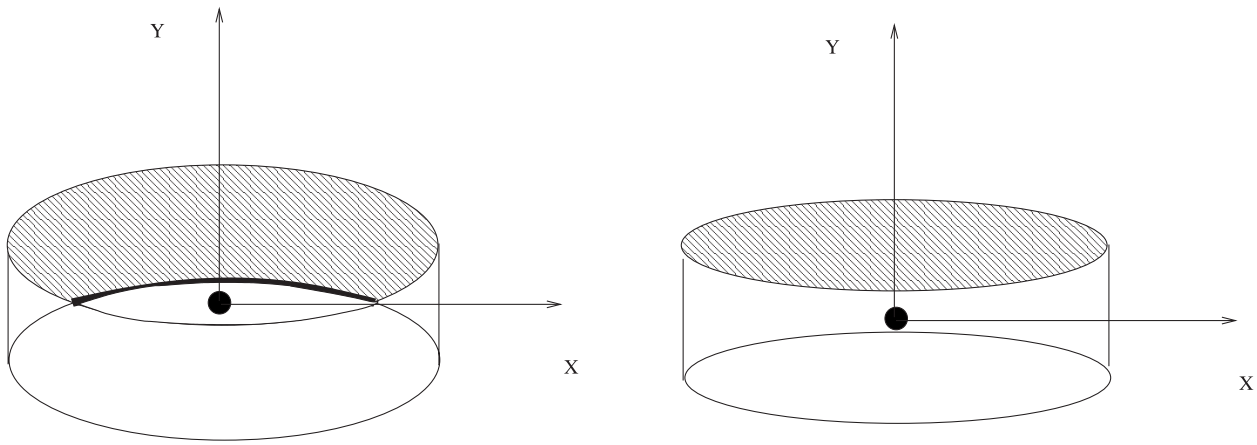

FIG. 9.—Schematic representation of the visible surface of the wall (*hatched surface*) as seen by the observer for two inclination angles, one corresponding to $\delta < 1$ (the star is visible) and the other one to $\delta > 1$ (the star is invisible).

Both ellipses intersect at critical angles: θ_c and $\pi - \theta_c$, where θ_c is given by

$$-(\cos i)(\sin\theta_c) + \frac{H}{R_d}\sin i = (\cos i)(\sin\theta_c) - \frac{H}{R_d}\sin i, \tag{37}$$

$$\sin\theta_c = \frac{H}{R_d}\tan i = \delta. \tag{38}$$

Depending on the inclination angle i, both ellipses can intersect if $\delta < 1$ or not if $\delta > 1$ (see Fig. 9). If $\delta > 1$, then the integration region is defined by the upper ellipse and $Y^-_{\rm up} < Y < Y^+_{\rm up}$, $0 < \theta < \pi$. If $\delta < 1$ there are two regions: if $0 < \theta < \arcsin\delta$, then $Y^-_{\rm up} < Y < Y^+_{\rm up}$; but if $\arcsin\delta < \theta < \pi/2$, then $Y^-_{\rm up} < Y < Y^+_{\rm down}$.

REFERENCES

Backman, D. E., Gillett, F. C., & Low, F. J. 1986, Adv. Space Res., 6, 43
Baraffe, I., Chabrier, G., Allard, F., & Hauschildt, P. H. 1998, A&A, 337, 403
Batalha, C., Batalha, N. M., Alencar, S. H. P., Lopes, D. F., & Duarte, E. S. 2002, ApJ, 580, 343
Bate, M. R., Bonnell, I. A., & Bromm, V. 2003, MNRAS, 339, 577
Begemann, B., Dorschner, J., Henning, T., Mutschke, H., & Thamm, E. 1994, ApJ, 423, L71
Bouwman, J., de Koter, A., Dominik, C., & Waters, L. B. F. M. 2003, A&A, 401, 577
Bruzual A., G., & Charlot, S. 1993, ApJ, 405, 538
Burns, J. A., Lamy, P. L., & Soter, S. 1979, Icarus, 40, 1
Calvet, N., D'Alessio, P., Hartmann, L., Wilner, D., Walsh, A., & Sitko, M. 2002, ApJ, 568, 1008
Calvet, N., Magris, G., Patiño, A., & D'Alessio, P. 1992, Rev. Mex. AA, 24, 27
Calvet, N., Muzerolle, J., Briceño, C., Hernández, J., Hartmann, L., Saucedo, J. L., & Gordon, K. D. 2004, AJ, 128, 1294
Calvet, N., Patiño, A., Magris, G., & D'Alessio, P. 1991, ApJ, 380, 617 (CPMD91)
Chen, C. H., & Jura, M. 2001, ApJ, 560, L171
Cohen, M., & Kuhi, L. V. 1979, ApJS, 41, 743
D'Alessio, P., Calvet, N., Hartmann, L., Lizano, S., & Cantó, J. 1999, ApJ, 527, 893
Dorschner, J., Begemann, B., Henning, T., Jäger, C., & Mutschke, H. 1995, A&A, 300, 503
Dorschner, J., Friedemann, C., Guertler, J., & Henning, T. 1988, A&A, 198, 223
Draine, B. T. 2003, ARA&A, 41, 241
Draine, B. T., & Lee, H. M. 1984, ApJ, 285, 89
Dullemond, C. P., Dominik, C., & Natta, A. 2001, ApJ, 560, 957
Duschl, W. J. 1989, MNRAS, 240, 219
Forrest, W. J., et al. 2004, ApJS, 154, 443
Hartmann, L. 2003, ApJ, 585, 398
Henning, T., & Mutschke, H. 1997, A&A, 327, 743
Henning, Th., Il'in, V. B., Krivova, N. A., Michel, B., & Voshchinnikov, N. V. 1999, A&AS, 136, 405
Indebetouw, R., et al. 2005, ApJ, 619, 931
Jäger, C., Mutschke, H., Begemann, B., Dorschner, J., & Henning, T. 1994, A&A, 292, 641
Jura, M., Zuckerman, B., Becklin, E. E., & Smith, R. C. 1993, ApJ, 418, L37
Kenyon, S. J., Brown, D. I., Tout, C. A., & Berlind, P. 1998, AJ, 115, 2491
Kenyon, S. J., Dobrzycka, D., & Hartmann, L. 1994, AJ, 108, 1872
Kenyon, S. J., & Hartmann, L. 1995, ApJS, 101, 117 (KH95)
Lutz, D. 1999, in The Universe as Seen by ISO, ed. P. Cox, & M. F. Kessler (ESA SP-427; Noordwijk: ESA), 623
Marsh, K. A., & Mahoney, M. J. 1992, ApJ, 395, L115
———. 1993, ApJ, 405, L71
Mathieu, R. D., Ghez, A. M., Jensen, E. L. N., & Simon, M. 2000, in Protostars and Planets IV, ed. V. Mannings, A. P. Boss, & S. S. Russell (Tucson: Univ. Arizona Press), 703
Mathis, J. S., Rumpl, W., & Nordsieck, K. H. 1977, ApJ, 217, 425
Mihalas, D. 1978, Stellar Atmospheres (2nd ed.; San Francisco: Freeman)
Moneti, A., Stolovy, S., Blommaert, J. A. D. L., Figer, D. F., & Najarro, F. 2001, A&A, 366, 106
Muzerolle, J., Calvet, N., Briceño, C., Hartmann, L., & Hillenbrand, L. 2000, ApJ, 535, L47
Muzerolle, J., Calvet, N., Hartmann, L., & D'Alessio, P. 2003, ApJ, 597, L149
Ossenkopf, V., Henning, T., & Mathis, J. S. 1992, A&A, 261, 567
Osterloh, M., & Beckwith, S. V. W. 1995, ApJ, 439, 288
Pascucci, I., Wolf, S., Steinacker, J., Dullemond, C. P., Henning, T., Niccolini, G., Woitke, P., & Lopez, B. 2004, A&A, 417, 793
Pollack, J. B., Hollenbach, D., Beckwith, S., Simonelli, D. P., Roush, T., & Fong, W. 1994, ApJ, 421, 615
Quillen, A. C., Blackman, E. G., Frank, A., & Varnière, P. 2004, ApJ, 612, L137
Rice, W. K. M., Wood, K., Armitage, P. J., Whitney, B. A., & Bjorkman, J. E. 2003, MNRAS, 342, 79
Siess, L., Dufour, E., & Forestini, M. 2000, A&A, 358, 593
Simpson, J. P. 1991, ApJ, 368, 570
Sitko, M. L., Lynch, D. K., & Russell, R. W. 2000, AJ, 120, 2609
Strom, K. M., Strom, S. E., Edwards, S., Cabrit, S., & Skrutskie, M. F. 1989, AJ, 97, 1451
Takeuchi, T., & Artymowicz, P. 2001, ApJ, 557, 990

Uchida, K. I., et al. 2004, ApJS, 154, 439
Webb, R. A., Zuckerman, B., Platais, I., Patience, J., White, R. J., Schwartz, M. J., & McCarthy, C. 1999, ApJ, 512, L63
Wiscombe, W. J. 1979, Mie Scattering Calculations: Advances in Technique and Fast, Vector-Speed Computer Codes, NCAR T/N-40+STR (Boulder: NCAR)
Wuchterl, G., Guillot, T., & Lissauer, J. J. 2000, Protostars and Planets IV, ed. V. Mannings, A. P. Boss, & S. S. Russell (Tucson: Univ. Arizona Press), 1081